Intensified Sulfite Reduction of Alkyl Hydroperoxides in a Rotor-Stator Spinning-Disc Reactor

I&EC research
Industrial & Engineering Chemistry Research
pubs.acs.org/IECR
Article

Intensified Sulfite Reduction of Alkyl Hydroperoxides in a Rotor–Stator Spinning-Disc Reactor

Maurilio Magosso, Laura J.W. Hazen, Michel van den Berg, and John van der Schaaf*

Cite This: *Ind. Eng. Chem. Res.* 2021, 60, 15540–15548
Read Online
ACCESS | Metrics & More | Article Recommendations

ABSTRACT: The reduction of *tert*-butyl hydroperoxide and cumene hydroperoxide with sodium metabisulfite was intensified in a rotor–stator spinning-disc reactor (rs-SDR). The reaction kinetics were first obtained in a capillary microreactor. The effects of temperature, aqueous phase ionic strength, mass transfer, and liquid–liquid interfacial area were quantified. A kinetic model was developed, and the kinetic parameters were fitted to the experimental data from the microreactor. *tert*-Butyl hydroperoxide could be reduced much faster than cumene hydroperoxide because of its higher solubility in the aqueous phase. The reduction rate in the rs-SDR was a factor 15–100 higher than that in the microreactor for rotational disc speeds of 1000–4500 rpm, respectively. This was entirely attributed to the increase in liquid–liquid interfacial area in the rs-SDR, which increased approximately linearly with rotational speed.

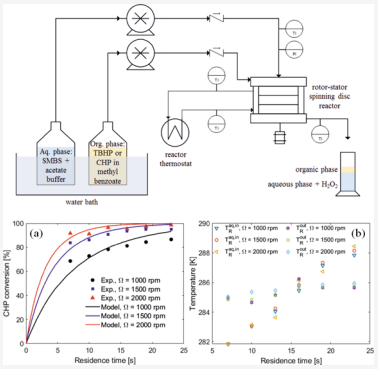

INTRODUCTION

Organic hydroperoxides are important compounds with different industrial applications. Tertiary alkyl- or arylalkyl hydroperoxides (AHPs) are the most employed and commercialized. These are used as curing agents for resins, in emulsion polymerizations, and as starting materials for the synthesis of more complex organic peroxides.[1,2] Organic hydroperoxides are readily reduced to the corresponding alcohols by many reagents like sodium hydrogensulfite, lithium aluminum hydride, sodium iodide, sodium thiosulfate, dimethyl sulfide, and triphenylphosphine.[3] This reaction is used for the synthesis of alcohols but also as a way to remove undesired hydroperoxide impurities. Since tertiary hydroperoxides are building blocks for the synthesis of peroxyesters, an undesired small amount of them is often present in the product. The peroxyester is thus washed with an aqueous bisulfite solution to reduce the hydroperoxide and increase the product purity.[4,5] Similar to the other process steps of peroxyester production, this operation is usually carried out in batch or fed-batch mode.[3] The goal of this work is to assess the possibility of performing the washing step continuously and to intensify it to reduce the total production process volume and reduce the risks involved with peroxides. First, we investigate the kinetics of AHP reduction in a transparent capillary microreactor. The reactions involved are presented in Scheme 1.

The effects of temperature, ionic strength, and interfacial area on the reaction rate were investigated in detail in this work. The use of the microreactor allowed an efficient temperature control and the determination of the specific interfacial area between the two liquid phases.[6] A kinetic model for the AHP reduction was developed in Matlab. The only available intensification study on the reduction of hydroperoxides focused on the use of static micromixers as reactors.[5] However, these devices have low productivity, are difficult to scale up, and do not allow for the separate control of shear rate and flowrate. In this work, the AHP reduction was performed in a three-stage rotor–stator spinning-disc reactor (rs-SDR), a novel type of high-shear reactor designed for the intensification of heterogeneous reactions by enhancing mass transfer and interfacial areas,[7−9] which does not present these limitations. The effect of the rotational speed on the reduction rate was

Scheme 1. Reactions Involved in the Alkyl Hydroperoxide (AHP) Reduction with Sodium Metabisulfite

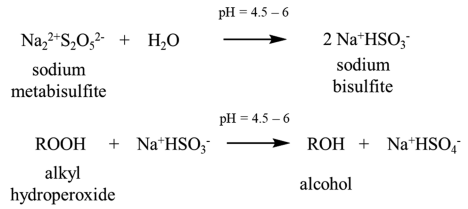

Received: August 19, 2021
Revised: October 11, 2021
Accepted: October 11, 2021
Published: October 22, 2021

https://doi.org/10.1021/acs.iecr.1c02626
Ind. Eng. Chem. Res. 2021, 60, 15540–15548

Scheme 2. Microreactor Setup for the Kinetic Study of the AHP Reduction

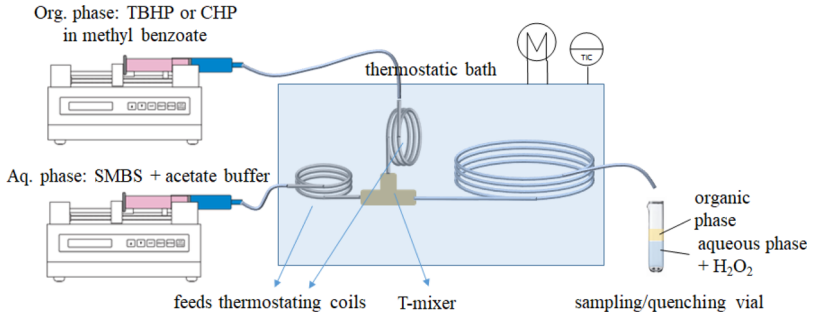

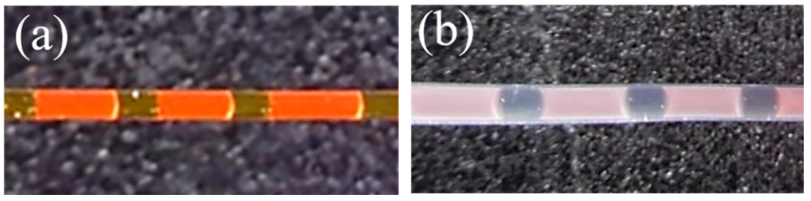

Figure 1. Picture of the slug-flow in an (a) FS capillary and (b) PFA capillary.

Scheme 3. rs-SDR Setup Used for the Intensification of the AHP Reduction

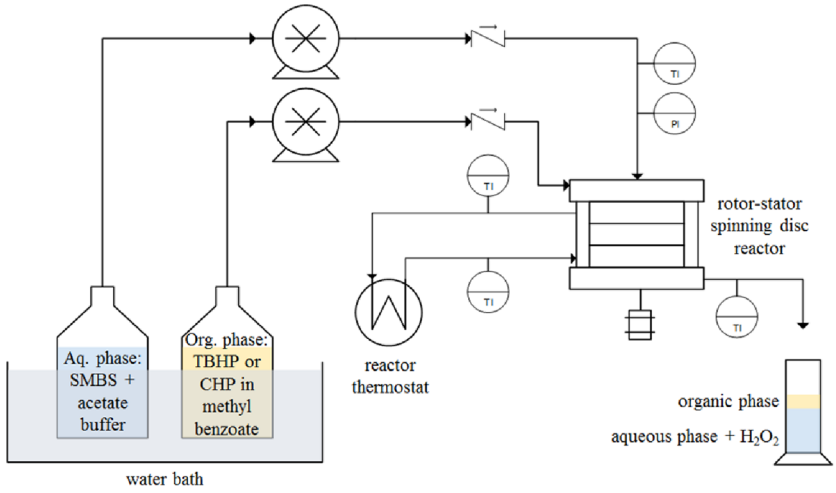

investigated, and the results were compared with those obtained in the microreactor.

EXPERIMENTAL SECTION

Materials. To simulate the washing step, methyl benzoate was used as the organic solvent instead of the peroxyester and a small amount of AHP was added to it. The mixture was contacted with an aqueous solution of sodium metabisulfite (SMBS) containing an acetate buffer. The acetate buffer was added to keep the pH between 4.5 and 6. In this range, most of the S(IV) is present as bisulfite ion HSO_3^-.[10] The reduction of two different tertiary AHPs was studied: *tert*-butyl hydroperoxide (TBHP) and cumene hydroperoxide (CHP). They are most commonly used in the synthesis of peroxyesters.[1] *tert*-Butyl hydroperoxide (70 wt % aqueous solution) was obtained from Alfa Aesar. Sodium acetate (anhydrous, ≥99%), sodium metabisulfite (98.0−100%), hydrogen peroxide (30% aqueous solution), and cumene hydroperoxide (80% solution in cumene) were purchased from Merck. Methyl benzoate (99%) and acetic acid (glacial, ≥99%) were from Sigma Aldrich. The exact assay of TBHP and CHP was determined by iodometric titration. The organic phase consisted of a 0.1 M solution of TBHP or CHP in methyl benzoate. The aqueous phase was prepared by dissolving sodium metabisulfite, sodium acetate, and acetic acid in water. Sodium acetate and acetic acid were added in the amount and proportion needed to have a starting pH of 6 and end up at pH ≅ 4.5 at complete hydroperoxide conversion. Without a buffer, the pH would drop more because of $NaHSO_4$ formation. To ensure the complete AHP reduction, sodium metabisulfite was added in excess with respect to AHP. The excess is given later on as the molar flow ratio of sodium bisulfite with respect to AHP, ϕ_{SBS}, considering that 1 mol of SMBS reacts with water to form 2 mol of SBS.

Microreactor Setup. The experimental setup is depicted in Scheme 2.

The organic and aqueous phases were loaded into two syringe pumps (Chemyx Fusion 500) and fed to the reaction capillary, where a liquid−liquid slug-flow pattern was formed. The capillaries were immersed in a thermostatic bath for precise temperature control. Both feed capillaries consisted of a metal coil (ID_{cap} = 0.75 × 10^{-3} m, OD_{cap} = 1.59 × 10^{-3} m, and

https://doi.org/10.1021/acs.iecr.1c02626
Ind. Eng. Chem. Res. 2021, 60, 15540−15548

$L_{cap} = 70 \times 10^{-2}$ m) to ensure that the two phases reached the desired temperature before they mixed. Depending on the experiment, the reaction capillary was made of SS or PFA and its inner diameter varied between 0.50×10^{-3} and 1.00×10^{-3} m. Pictures of the slug-flow were taken with a Nikon Coolpix A900 digital camera and used to determine the values of liquid−liquid interfacial area by manual image analysis. With the stainless steel capillary, a short piece of transparent fused silica (FS) capillary ($ID_{cap} = 0.75 \times 10^{-3}$ m, $OD_{cap} = 0.88 \times 10^{-3}$ m, and $L_{cap} = 6 \times 10^{-2}$ m) was connected to the end of the stainless steel capillary to take the slug-flow picture. Two samples of the slug-flow pictures are given in Figure 1.

For the two experiments of Figure 5a in which the diameter of the SS capillary was different than the diameter of the FS capillary at its end, the specific interfacial area in the SS capillary was calculated indirectly. The organic phase droplets in the SS capillary were assumed cylinders with the same volume of the droplets in the FS capillary, which was measured. The slug-flow characteristics varied in each experiment as a function of the hydroperoxide type and ID_{cap}. For all other parameters (capillary length, residence time, temperature, ionic strength, and slug-flow velocity), it was verified that the change in this parameter did not affect the slug-flow geometry and regularity.

Rotor−Stator Spinning-Disc Reactor Setup. The rs-SDR setup is reported in Scheme 3.

The temperature of the reactor thermostat was set to 283 K. The aqueous and organic phase bottles were immersed in a large volume water bath in which the temperature was manually adjusted to 278−283 K by adding ice. When the temperature of the reactants was equal to that of the bath, the experiment was started. The aqueous phase was pumped using a Tuthill D-series gear pump and the organic phase was pumped by means of a Cole-Parmer Masterflex L/S peristaltic pump with an Easy-Load II pump head. The feed lines were insulated with foam to limit the temperature rise of the pumped liquids. The two streams met at the center of the first disc of the rs-SDR and the reaction mixture came out from the bottom of the third disc. Four thermocouples were installed: one at the aqueous phase reactor inlet, one at the reactor outlet, one at the cooling jacket inlet, and one at the cooling jacket outlet. A vertical cross section of the reactor is set out in Figure 2.

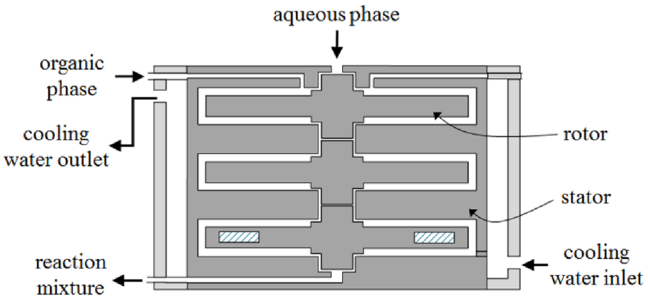

Figure 2. Vertical cross section of the rs-SDR.

The rs-SDR used was the SpinPro R-10 manufactured by Flowid with a customized cooling jacket. It consists of three rotating discs (rotors) enclosed by a housing with three cylindrical cavities (stator). The rotation was imparted to the disc via magnetic coupling, and a range between 1000 and 8000 rpm was chosen. The disc diameter was 7 cm, the distance between the disc surface and the housing was 0.5 mm, and the space between the disc rim and the stator wall was 1 mm. The total reactor volume was 19 mL, corresponding to a single stage volume of 6.3 mL. Every component of the reactor was made of silicon carbide. The exceptional heat conductivity of this material ($K_{T,\,SiC} = 490$ W m^{-1} K^{-1}) ensures a high heat exchange performance and uniform reaction conditions.

Analytical Methods. For the microreactor experiments, the reaction mixture was collected in a vial containing 5.0 mL of a 2 M H_2O_2 aqueous solution until ca. 1.5 mL of the organic phase was present. With the SDR, a cylinder containing 50 mL of the 2 M H_2O_2 aqueous solution was used instead and the reaction mixture was collected until 15 mL of the organic phase accumulated. The separation of the reaction mixture in the receiving containers was very quick, and the H_2O_2 served as the quenching agent by oxidizing all the SBS present in the aqueous phase before it could further react with AHP. The organic phase (1.0 mL) was withdrawn with a micropipette and diluted to 10 mL with methanol in a volumetric flask.

The hydroperoxide concentration was determined with a Shimadzu HPLC equipped with a CBM-20A controller, two LC-20 AD XR pumps, a 193 SIL-20 AC XR autosampler, a CTO-20 AC column oven, and an SPD-M20AD diode array detector. An Agilent ZORBAX SB-C18, 4.6 × 250 mm, 5 μm column was used. The eluent consisted of a mixture of water (35 vol %) and methanol (65 vol %) with 0.01 M phosphoric acid to ensure the protonation of the hydroperoxides and avoid double peaks in the chromatogram. During each analysis, the composition of the eluent was kept constant. The eluent flowrate was 1 mL/min, and the injection volume was 5 μL. A diode array detector was used, and the chromatograms were acquired at a wavelength of 210 nm. The hydroperoxide concentration in the aqueous phase was not measured since it was lower than the detection limits of the instrument and therefore negligible compared to its concentration in the organic phase.

Knowing the hydroperoxide concentration in the organic phase at the reactor outlet and inlet, the hydroperoxide conversion could be determined:

$$X_{AHP} = 1 - \frac{C_{AHP}^{org,out}}{C_{AHP}^{org,in}} \quad (1)$$

The previous calculation assumes that the organic phase volumetric flowrate does not change during the reaction. The assumption is valid because the amount of AHP initially present in the organic phase is very low.

RESULTS AND DISCUSSION

Microreactor Experiments. For each graph of AHP conversion, the experimental value of the specific interfacial area a is given. This value corresponds to the average of the interfacial areas measured for each experimental point shown in the plot. The standard deviation of the a values is also indicated and was always less than 10% of the average value. The effect of the two most important variables for the reduction of both TBHP and CHP, residence time and temperature, was investigated first. Figure 3 shows the conversion of AHP (X_{AHP}) versus the residence time at several temperatures.

It is clear that TBHP is more reactive than CHP due to its higher solubility in the aqueous phase, where the reducing agent resides, and probably also due to its higher intrinsic

https://doi.org/10.1021/acs.iecr.1c02626
Ind. Eng. Chem. Res. 2021, 60, 15540−15548

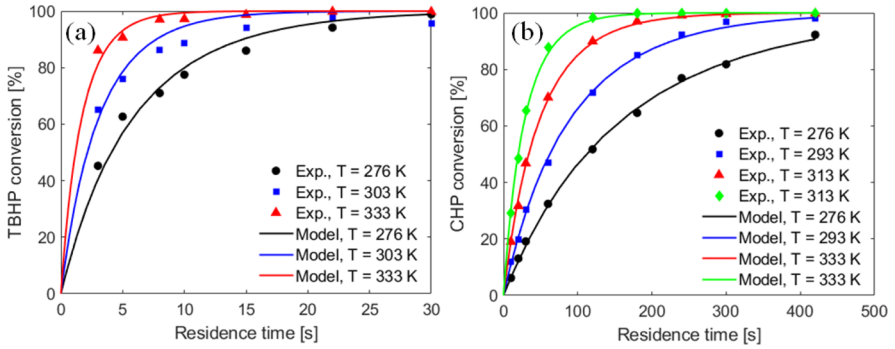

Figure 3. Organic hydroperoxide conversion vs residence time at several temperatures for (a) TBHP, $a = 4218 \pm 338$ m^{-1} and (b) CHP, $a = 4641 \pm 287$ m^{-1}. Experimental conditions: $C_{AHP}^{org,\,in} = 0.100$ M, $C_{SMBS}^{aq,\,in} = 0.225$ M, $A/O = 0.55$, $\phi_{SBS} = 2.4$, $ID_{cap} = 0.75 \times 10^{-3}$ m, and SS capillary. The solid lines represent the fitting obtained using the model of eq 12.

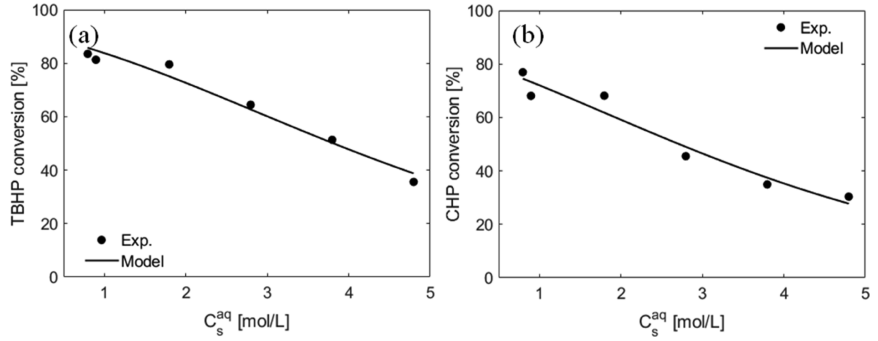

Figure 4. Effect of ionic strength on the AHP reduction rate for (a) TBHP, $\tau = 10$ s, $a = 4218 \pm 338$ m^{-1} and (b) CHP, $\tau = 180$ s, $a = 4641 \pm 287$ m^{-1}. Experimental conditions: $T = 283$ K, $C_{AHP}^{org,\,in} = 0.100$ M, $C_{SMBS}^{aq,\,in} = 0.225$ M, $A/O = 0.55$, $\phi_{SBS} = 2.4$, $ID_{cap} = 0.75 \times 10^{-3}$ m, and SS capillary. The solid lines represent the fitting obtained using the model of eq 12.

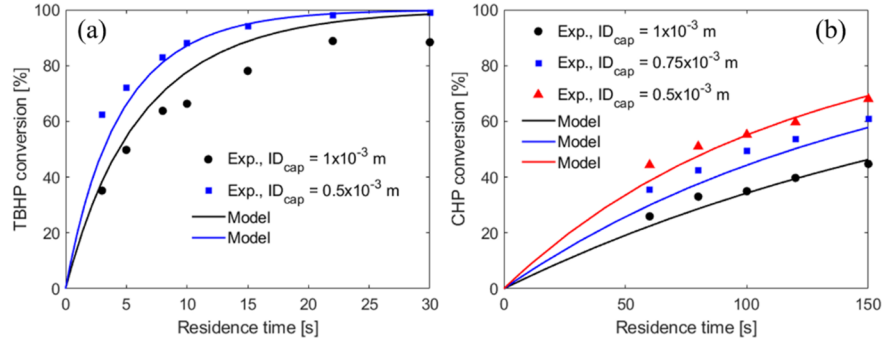

Figure 5. Effect of interfacial area on the AHP reduction rate for (a) TBHP, $T = 283$ K, SS capillary, black circle $a = 3506 \pm 178$ m^{-1}, blue square $a = 4917 \pm 289$ m^{-1}; (b) CHP, $T = 293$ K, PFA capillary, red triangle $a = 3302 \pm 360$ m^{-1}, blue square $a = 2384 \pm 180$ m^{-1}, black circle $a = 1693 \pm 81$ m^{-1}. Experimental conditions: $C_{AHP}^{org,\,in} = 0.100$ M, $C_{SMBS}^{aq,\,in} = 0.225$ M, $A/O = 0.55$, and $\phi_{SBS} = 2.4$. The solid lines represent the prediction obtained using the model of eq 12 with the parameters from Table 1.

reactivity. To quantify the solubility effect, the partition coefficients of both hydroperoxides were determined by stirring the organic phase, with AHP, together with the aqueous phase, without SMBS, for 30 min at 293 K and measuring the hydroperoxide concentration in both phases. The CHP concentration in the aqueous phase was under the detection limit of the HPLC; therefore, it was determined using ^{1}H NMR spectroscopy. The resulting partition coefficients were $K_{p,\,TBHP} = 2 \times 10^{-1}$ m_{aq}^3/m_{org}^3 and $K_{p,\,CHP} = 1.75 \times 10^{-2}$ m_{aq}^3/m_{org}^3, indicating that TBHP is approximately 10 times more soluble in the aqueous phase than CHP. Increasing the temperature leads to a higher intrinsic kinetic constant and a lower AHP solubility in the aqueous phase.[11,12] These two effects counteract each other, but the influence of temperature on the kinetic constant is higher, so the reaction rate increases with temperature.

The partition coefficient is also influenced by the ionic strength of the aqueous phase. Due to the salting-out effect, the organic compound solubility reduces in aqueous solutions containing electrolytes. The partition coefficient is described by the Setschenow equation:[13−16]

$$\ln \frac{K_{p,AHP}}{K_{p,AHP}^0} = -k_s C_s^{aq} \tag{2}$$

where $K_{p,\,AHP}^0$ is the AHP partition coefficient at $C_s^{aq} = 0$, $K_{p,\,AHP}$ is the partition coefficient at any ionic strength, k_s the Setschenow constant, and C_s^{aq} the total salt concentration in

https://doi.org/10.1021/acs.iecr.1c02626
Ind. Eng. Chem. Res. 2021, 60, 15540−15548

the aqueous phase. The effect of the ionic strength was checked with an experiment in which the AHP conversion at a constant residence time was determined for different aqueous phase ionic strengths, obtained by adding different amounts of NaCl, shown in Figure 4.

The ionic strength is expressed as C_S^{aq}, which is the total salt concentration of the aqueous phase, including SBS, sodium acetate from the pH buffer, and the added NaCl. The AHP conversion decreases with the increase of C_S^{aq}, as expected from eq 2.

Another parameter that commonly affects liquid−liquid heterogeneous reaction rates is the interfacial area. This variable can be changed by using capillaries with different inner diameters.[17,18] The narrower the capillary is, the higher is the interfacial area. Figure 5 shows the reduction rates obtained for TBHP and CHP in capillaries of different sizes, with the corresponding interfacial areas.

Clearly, a larger interfacial area increases the reaction rate. Combined with the observed fast reaction rates, this suggests the presence of mass-transfer limitations. To better elucidate the kinetic mechanism, an additional check was carried out by determining the influence of the slug-flow velocity on the AHP reduction since it is known that, for liquid−liquid mass-transfer limited reactions in slug-flow microreactors, an increase in the velocity leads to a higher degree of mixing and mass transfer and, consequently, higher reaction rates.[17,19] While the velocity was modified, the residence time was kept constant by changing the capillary length accordingly. Figure 6 remarkably shows that the velocity had no influence on the fastest reaction rate.

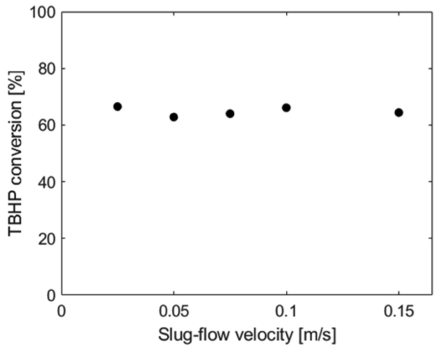

Figure 6. Effect of slug-flow velocity on the TBHP reduction rate. Experimental conditions: T = 283 K, τ = 4 s, $C_{AHP}^{org,\,in}$ = 0.100 M, $C_{SMBS}^{aq,\,in}$ = 0.225 M, a = 4218 ± 338 m^{-1}, A/O = 0.55, ϕ_{SBS} = 2.4, ID_{cap} = 0.75 × 10^{-3} m, and SS capillary.

This result can be explained by assuming the concentration profile depicted in Figure 7.

These concentration profles are based on the following assumptions:

- reduction reaction is very fast and takes place entirely in the boundary layer of the aqueous phase;
- AHP and SBS concentrations in the film of the organic and aqueous phase, respectively, are equal to their concentration in the bulk; i.e., the reaction rate is much slower than the mass transfer to the interface.

The corresponding reaction rate will then not depend on mass transfer but still will be proportional to the specific interfacial area a (see also eq 3, Kinetic Modeling section).

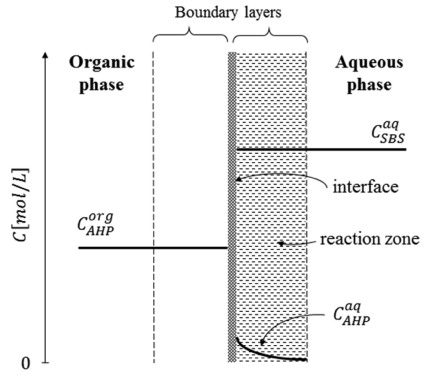

Figure 7. Proposed concentration profiles for the AHP reduction.

Rotor−Stator Spinning Disc Reactor Experiments. The influence of residence time and disc rotational speed was investigated in the rs-SDR. The effect on the CHP reduction rate is reported in Figures 8 and 9. The corresponding inlet and outlet reactor temperatures are also depicted in those figures. The inlet and outlet temperatures of the cooling jacket are always 283 ± 1 K, the set-point temperature of the reactor thermostat. This was achieved by the high capacity of the thermostat and the high flowrate of cooling liquid.

An equivalent experiment using TBHP and a residence time of 7 s resulted in 100% conversion at every rotational speed. For CHP, it is evident that, even at the lowest rotational speed of 1000 rpm, the reduction rate in the SDR is ca. 8× faster as a result of the higher liquid−liquid interfacial area. When the rotational speed was increased, the interfacial area also increased and so did the CHP conversion. Figure 8b shows that $T_R^{aq,\,in}$ is approximately 286 K. $T_R^{aq,\,in}$ increases with residence time due to the increased warming up of the reactants in the feeding tubes. T_R^{out} increases from 284.5 K at 1000 rpm to 288 K at 4500 rpm; the temperature rises due to the increased friction at higher rotational speeds.

KINETIC MODELING

A kinetic model was developed on the basis of the experimental results and observations. The assumed kinetic regime corresponds to the concentration profiles depicted in Figure 7. For this interface behavior (fast reaction in the film and high AHP and SBS concentrations), the AHP reduction rate reduces to a pseudo-first-order equation:[20]

$$R_r = C_{AHP}^{org} a \sqrt{K_{p,AHP}{}^2 \mathcal{D}_{AHP}^{aq} k_r C_{SBS}^{aq}} \quad (3)$$

where $\mathcal{D}_{AHP}^{aq}$ is the diffusion coefficient of AHP in the aqueous phase and k_r is the intrinsic kinetic rate constant. As shown in the results section, $K_{p,\,AHP}$ depends on the aqueous phase ionic strength following eq 2. $K_{p,\,AHP}^0$, $\mathcal{D}_{AHP}^{aq}$, and k_R are influenced by temperature. The AHP partition is related to the Gibbs energy, the molar enthalpy, and the molar entropy of the association equilibrium between the compositions of a component in two liquids[11] by the following equations:

$$\Delta_{tr}G^0 = 2.303RT \ln K_{p,AHP}^0 \quad (4)$$

$$\Delta_{tr}G^0 = \Delta_{tr}H^0 - T\Delta_{tr}S^0 \quad (5)$$

By combining eqs 4 and 5, we obtain:

https://doi.org/10.1021/acs.iecr.1c02626
Ind. Eng. Chem. Res. 2021, 60, 15540−15548

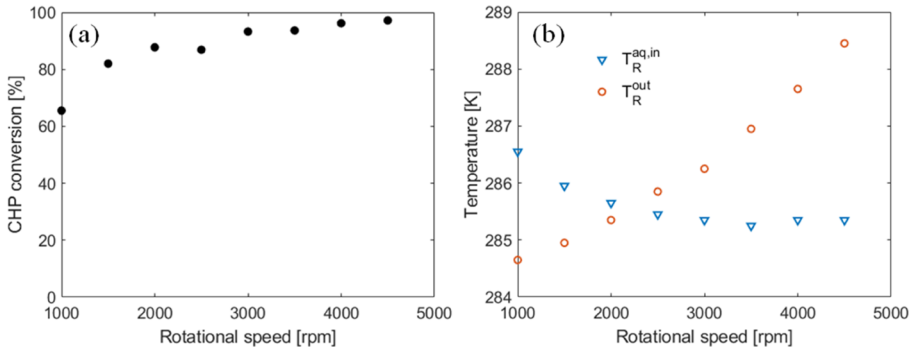

Figure 8. Effect of rotational speed on (a) CHP conversion and (b) inlet/outlet reactor temperatures of the SDR. Experimental conditions: $C_{AHP}^{org,\,in}$ = 0.100 M, $C_{SMBS}^{aq,\,in}$ = 0.225 M, τ = 7 s, A/O = 0.55, and ϕ_{SBS} = 2.4.

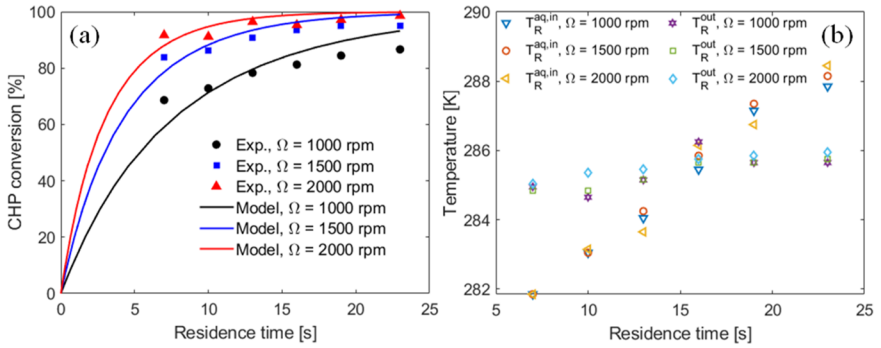

Figure 9. Effect of rotational speed and residence time on the (a) CHP conversion and (b) inlet/outlet reactor temperatures of the SDR. Experimental conditions: $C_{AHP}^{org,\,in}$ = 0.100 M, $C_{SMBS}^{aq,\,in}$ = 0.225 M, A/O = 0.55, and ϕ_{SBS} = 2.4. The solid lines represent the fitting obtained using the model of eq 12 with the parameters from Table 1.

$$K_{p,AHP}^{0} = B\exp\left(\frac{\Delta_{tr}H^{0}}{2.303RT}\right) \tag{6}$$

where $B = \exp\left(-\frac{\Delta_{tr}S^{0}}{2.303R}\right)$ is a constant.

The temperature dependence of the diffusion coefficient is given by:[21]

$$\mathcal{D}_{AHP}^{aq} = C\exp\left(-\frac{Q}{T}\right) \tag{7}$$

where C and Q are constants.

Finally, to take the effect of temperature on the kinetic constant k_r into account, the Arrhenius expression is used:

$$k_r = A_r\exp\left(-\frac{E_{a,r}}{RT}\right) \tag{8}$$

By combining eqs 2, 6, 7, and 8, eq 3 can be rewritten as:

$$R_r = \sqrt{A_r^{*}\exp\left(-\left(\frac{E_{a,r}^{*}}{RT} + 2k_sC_s^{aq}\right)\right)C_{SBS}^{aq}\,C_{AHP}^{org}a} \tag{9}$$

where A_r^{*} and $E_{a,\,r}^{*}$ are the apparent pre-exponential factor and activation energy of the reduction reaction equal to:

$$A_r^{*} = {K_{p,AHP}^{0}}^{2}AB^{2}C \tag{10}$$

$$E_{a,r}^{*} = E_{a,r} + QR - \frac{2}{2.303}\Delta_{tr}H^{0} \tag{11}$$

The mole balance of a PFR was used to simulate the microreactor and the SDR:

$$\frac{dC_{AHP}^{org}}{d\tau} = -\frac{R_r}{\theta^{org}} \tag{12}$$

The model was implemented in Matlab using the ODE15s function to solve the mole balances. The parameters A_r^{*}, $E_{a,\,r}^{*}$, and k_s, which are presented in Table 1 for both TBHP and CHP, were fitted from the microreactor experiments reported in Figures 3 and 4 using the Lsqcurvefit function. The calculated values from the fitting are shown in solid lines in the same figures. The obtained apparent activation energies are close, indicating a similar temperature dependence of the reduction rates for TBHP and CHP. A deeper investigation would be needed to find out which terms of eq 11 have a predominant effect on the temperature dependence. On the other hand, the fitted apparent pre-exponential factor A_r^{*} is higher for TBHP with respect to CHP. Most likely, this difference is mainly due to the value of the partition coefficient K_p^0, which is higher for TBHP. While the partition coefficients of the two compounds are different, they change in a similar way with the aqueous phase ionic strength, as demonstrated by the close values of the Setschenow constants in Table 1.

Table 1. Fitted Kinetic Parameters for the AHP Reduction

AHP	A_r^{*}	$E_{a,\,r}^{*}$	k_s
TBHP	4.324×10^{-2}	3.820×10^{4}	3.681×10^{-1}
CHP	2.050×10^{-3}	4.637×10^{4}	3.784×10^{-1}

The model with the fitted parameters of Table 1 was used to predict the experimental results of the microreactor at different interfacial areas set out in Figure 5, where the predicted values are shown in solid lines. The model and the parameters

https://doi.org/10.1021/acs.iecr.1c02626
Ind. Eng. Chem. Res. 2021, 60, 15540−15548

determined from the microreactor experiments were also used to fit the interfacial areas created by the SDR using the data displayed in Figures 8a and 9a. Each experimental point depicted in Figure 8a, which corresponds to a different rotational speed, was fitted separately to determine the corresponding interfacial area. The fitting is therefore not reported. In Figure 9a, all the data obtained at the same rotational speed were fitted together and the fitting is represented by solid lines in the same figure. The determined values of a are given in Figure 10.

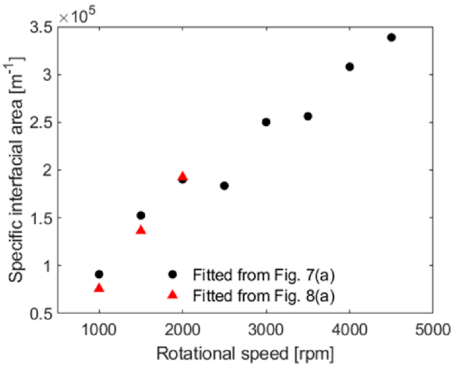

Figure 10. Specific interfacial areas in the SDR fitted from the experiments using the model of eq 12 with the parameters from Table 1.

Although the calculation only gives an estimation of the specific interfacial areas and cannot replace direct measurements, it can be observed that even at the lowest rotational speed of 1000 rpm, a is already 15 times larger than the highest value measured in the microreactor for CHP. At the highest rotational speed applied, a becomes 100 times larger. Moreover, the specific interfacial area appears to have a linear dependence on the rotational speed and probably increases further for rotational speeds higher than 4500 rpm. The increase in interfacial area is caused by the increase of shear force between the rotor and the stator with the rotational speed.[22]

The parity plot in Figure 11 shows that the agreement between the model and experiments is within ±90% confidence band.

The model line for the 1 mm capillary in Figure 5a is slightly off, possibly due to an inaccurate specific interfacial area measurement caused by the transition from the SS capillary with $ID_{cap} = 1.00 \times 10^{-3}$ m to the FS capillary piece with $ID_{cap} = 0.75 \times 10^{-3}$ m. In Figure 9a, the model tends to underestimate the experimental data at low residence times and overestimate them at high residence times. The most likely explanation for these deviations is that an increasing flowrate leads to an increase in the plug-flow region present in the experimental SDR and a smaller ideally stirred region,[23] leading to higher conversions at lower residence times due to the higher AHP concentrations present in the reactor.

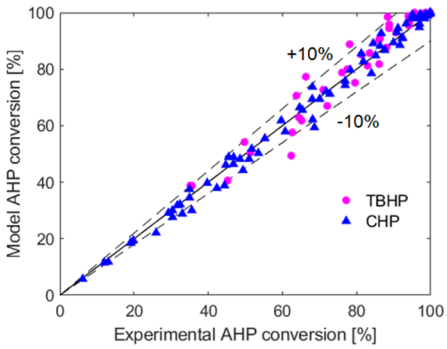

Figure 11. Comparison of the predicted and experimental AHP conversions in the microreactor.

CONCLUSIONS

The kinetics of the liquid−liquid sulfite reduction of TBHP and CHP are shown to take place in the aqueous phase by mass transfer of the AHP and the subsequent fast reaction with the sodium bisulfite present in the boundary layer near the interface. The reaction kinetics are adequately modeled taking into account the effect of interfacial area, temperature, and ionic strength. CHP is reduced more slowly than TBHP because of its lower solubility in the aqueous phase and probably lower reactivity. It was shown that the reaction rate increases with temperature and interfacial area and decreases with ionic strength. On the basis of these findings, the sulfate reduction of hydroperoxides was intensified using a rotor−stator spinning-disc reactor. The AHP reduction rate in the rs-SDR was up to 17 times larger than the microreactor reduction rate at a disc rotational speed of 4500 rpm due to a higher interfacial area caused by the large shear force. The reaction would probably become even faster for rotational speeds higher than 4500 rpm. However, such values could not be tested because full AHP conversion was already reached at 4500 rpm and it was not possible to further reduce the residence time and/or the temperature with the equipment used. The rs-SDR thus intensifies the AHP reduction significantly and enables one to perform the industrial removal of AHP from peroxyesters continuously in an intensified, efficient, and safe manner. Moreover, the reactor can be easily scaled up to meet the productivity requirements. The scale-up is achieved by using an rs-SDR with a larger disc radius with respect to the SpinPro R-10 reactor used in this study. With a disc radius of 6.6 cm and a gap between the disc surface and the stator of 1.1 mm, the disc volume per stage equals 63 mL. The reactor volume can be further increased by adding additional rotor−stator units in series, where the rotors are mounted on a common axis.[24]

AUTHOR INFORMATION

Corresponding Author

John van der Schaaf − *Sustainable Process Engineering, Department of Chemical Engineering and Chemistry, Eindhoven University of Technology, Eindhoven, MB 5600, The Netherlands;* Present Address: Sustainable Process Engineering, Department of Chemical Engineering and Chemistry, Eindhoven University of Technology, P.O. Box 513, 5600 MB Eindhoven, The Netherlands; orcid.org/0000-0002-2856-8592; Email: j.vanderschaaf@tue.nl

Authors

Maurilio Magosso − *Sustainable Process Engineering, Department of Chemical Engineering and Chemistry, Eindhoven University of Technology, Eindhoven, MB 5600, The Netherlands;* Present Address: Sustainable Process Engineering, Department of Chemical Engineering and

https://doi.org/10.1021/acs.iecr.1c02626
Ind. Eng. Chem. Res. 2021, 60, 15540−15548

Chemistry, Eindhoven University of Technology, P.O. Box 513, 5600 MB Eindhoven, The Netherlands

Laura J.W. Hazen − *Sustainable Process Engineering, Department of Chemical Engineering and Chemistry, Eindhoven University of Technology, Eindhoven, MB 5600, The Netherlands;* Present Address: Sustainable Process Engineering, Department of Chemical Engineering and Chemistry, Eindhoven University of Technology, P.O. Box 513, 5600 MB Eindhoven, The Netherlands

Michel van den Berg − *Sustainable Process Engineering, Department of Chemical Engineering and Chemistry, Eindhoven University of Technology, Eindhoven, MB 5600, The Netherlands;* Present Address: Nouryon, Polymer Catalysts, P.O. Box 10, 7400 AA Deventer, The Netherlands.

Complete contact information is available at: https://pubs.acs.org/10.1021/acs.iecr.1c02626

Author Contributions

The manuscript was written through contributions of all authors. All authors have given approval to the final version of the manuscript.

Funding

This research was carried out within the HighSinc program, a joint development between Nouryon Specialty Chemicals and the Department of Chemical Engineering and Chemistry from Eindhoven University of Technology.

Notes

The authors declare no competing financial interest.

■ ACKNOWLEDGMENTS

The authors would like to thank Lian Nabuurs and Andre Koolaard for the help in building the rotor−stator spinning-disc setup and the safety supervision. Many thanks also to Mihails Kulagins for the assistance on the analytics.

■ NOMENCLATURE

Latin Symbols

ID_{cap}	capillary inner diameter, m
OD_{cap}	capillary outer diameter, m
L_{cap}	capillary length, m
X	conversion, −
C	concentration, mol L^{-1}
a	liquid−liquid interfacial area per unit of reactor volume, m^2 m_R^{-3}
A/O	aqueous over organic volumetric flowrate ratio, −
$\dot{n}$	molar flowrate, mol s^{-1}
$K_{p,\,AHP}$	AHP partition coefficient at any C_s^{aq}, $C_{AHP}^{aq}/C_{AHP}^{org}$, m_{aq}^3/m_{org}^3
$K_{p,\,AHP}^0$	AHP partition coefficient at $C_s^{aq} = 0$, $C_{AHP}^{aq}/C_{AHP}^{org}$, m_{aq}^3/m_{org}^3
T	temperature, K
$\mathcal{D}$	diffusion coefficient, m^2 s^{-1}
R_r	reduction reaction rate, mol L^{-1} s^{-1}
k_r	reduction reaction kinetic constant, L mol^{-1} s^{-1}
k_S	Setschenow constant, L mol^{-1}
R	universal gas constant, J mol^{-1} K^{-1}
$\Delta_{tr}G^0$	Gibbs energy of transfer, J
$\Delta_{tr}H^0$	enthalpy of transfer, J
$\Delta_{tr}S^0$	entropy of transfer, J K^{-1}
A_r^*	apparent pre-exponential factor of the reduction reaction, m^2 L mol^{-1} s^{-2}
$E_{a,\,r}^*$	apparent activation energy of the reduction reaction, J mol^{-1}

Greek Symbols

ϕ_{SBS}	molar flow ratio of SBS with respect to AHP, $\dot{n}_{SBS}^{aq}/\dot{n}_{AHP}^{org}$
τ	residence time, s
θ	volumetric liquid holdup, −
Ω	disc rotational speed, rpm

Abbreviations

AHP	alkyl/arylalkyl hydroperoxide
SMBS	sodium metabisulfite
SBS	sodium bisulfite
TBHP	*tert*-butyl hydroperoxide
CHP	cumene hydroperoxide
SS	stainless steel
PFA	perfluoroalkoxy alkane
rs-SDR	rotor−stator spinning-disc reactor

Superscripts

org	organic phase
in	inlet
out	reactor outlet

Subscripts

S	salt
R	reactor

■ REFERENCES

(1) Uhl, A.; Bitzer, M.; Wolf, H.; Hermann, D.; Gutewort, S.; Völkl, M.; Nagl, I. Peroxy Compounds, Organic. In *Ullmann's Encyclopedia of Industrial Chemistry*; Wiley-VCH Verlag GmbH & Co. KGaA: Weinheim, Germany, 2018; pp. 1−45.

(2) Gilchrist, T. L. Reduction of NN, NN, NO and OO Bonds. In *Comprehensive Organic Synthesis*; Elsevier, 1991; pp. 381−402.

(3) Sanchez, J.; Myers, T. N. Peroxides and Peroxide Compounds, Organic Peroxides. In *Kirk-Othmer Encyclopedia of Chemical Technology*; John Wiley & Sons, Inc.: Hoboken, NJ, USA, 2000, p. 37.

(4) Uday, D. W.; Venkatram, R. Continuous Manufacture of Peroxyesters. US Pat., US 4,075,236 B1, 1978.

(5) Azzawi, A.; Mehesch, H.-E.; Von Zadow, E.; Kirsch, S.; Wormland, B.; Sondermann, M. Method for the Production of Organic Peroxides by Means of a Microreactor Techniques. US Pat., US 7,968,753 B2, 2011.

(6) Ufer, A.; Mendorf, M.; Ghaini, A.; Agar, D. W. Liquid/Liquid Slug Flow Capillary Microreactor. *Chem. Eng. Technol.* **2011**, *34*, 353−360.

(7) Meeuwse, M.; Van Der Schaaf, J.; Kuster, B. F. M.; Schouten, J. C. Gas − Liquid Mass Transfer in a Rotor − Stator Spinning Disc Reactor. *Chem. Eng. Sci.* **2010**, *65*, 466−471.

(8) Meeuwse, M.; Lempers, S.; van der Schaaf, J.; Schouten, J. C. Liquid−Solid Mass Transfer and Reaction in a Rotor−Stator Spinning Disc Reactor. *Ind. Eng. Chem. Res.* **2010**, *49*, 10751−10757.

(9) Visscher, F.; van der Schaaf, J.; de Croon, M. H. J. M.; Schouten, J. C. Liquid-Liquid Mass Transfer in a Rotor-Stator Spinning Disc Reactor. *Chem. Eng. J.* **2012**, *185-186*, 267−273.

(10) Robbin Martin, L.; Damschen, D. E. Aqueous Oxidation of Sulfur Dioxide by Hydrogen Peroxide at Low PH. *Atmos. Environ.* **1981**, *15*, 1615−1621.

(11) Noubigh, A.; Mgaidi, A.; Abderrabba, M. Temperature Effect on the Distribution of Some Phenolic Compounds: An Experimental Measurement of 1-Octanol/Water Partition Coefficients. *J. Chem. Eng. Data* **2010**, *55*, 488−491.

(12) Bahadur, N. P.; Shiu, W.-Y.; Boocock, D. G. B.; Mackay, D. Temperature Dependence of Octanol−Water Partition Coefficient for Selected Chlorobenzenes. *J. Chem. Eng. Data* **1997**, *42*, 685−688.

(13) Ni, N.; Yalkowsky, S. H. Prediction of Setschenow Constants. *Int. J. Pharm.* **2003**, *254*, 167−172.

(14) Xie, W.-H.; Shiu, W.-Y.; Mackay, D. A Review of the Effect of Salts on the Solubility of Organic Compounds in Seawater. *Mar. Environ. Res.* **1997**, *44*, 429−444.
(15) Ferreira, L. A.; Chervenak, A.; Placko, S.; Kestranek, A.; Madeira, P. P.; Zaslavsky, B. Y. Responses of Polar Organic Compounds to Different Ionic Environments in Aqueous Media Are Interrelated †. *Phys. Chem. Chem. Phys.* **2014**, *16*, 23347.
(16) Schröder, B.; Freire, M. G.; Varanda, F. R.; Marrucho, I. M.; Santos, L. M. N. B. F.; Coutinho, J. A. P. Aqueous Solubility, Effects of Salts on Aqueous Solubility, and Partitioning Behavior of Hexafluorobenzene: Experimental Results and COSMO-RS Predictions. *Chemosphere* **2011**, *84*, 415−422.
(17) Ghaini, A.; Kashid, M. N.; Agar, D. W. Effective Interfacial Area for Mass Transfer in the Liquid-Liquid Slug Flow Capillary Microreactors. *Chem. Eng. Process. Process Intensif.* **2010**, *49*, 358−366.
(18) Kashid, M. N.; Agar, D. W. Hydrodynamics of Liquid-Liquid Slug Flow Capillary Microreactor: Flow Regimes, Slug Size and Pressure Drop. *Chem. Eng. J.* **2007**, *131*, 1−13.
(19) Di, N.; Raimondi, M.; Prat, L.; Gourdon, C.; Cognet, P. Direct Numerical Simulations of Mass Transfer in Square Microchannels for Liquid − Liquid Slug Flow. *Chem. Eng. Sci.* **2008**, *63*, 5522−5530.
(20) Levenspiel, O. Fluid-Fluid Reactions: Kinetics. In *Chemical Reaction Engineering*; John Wiley & Sons, Inc.: New York, 1999; pp. 523−539.
(21) Poling, B. E.; Prausnitz, J. M.; O'connell, J. P. Diffusion Coefficients. In *The Properties of Gases and Liquids*; McGraw-Hill: New York, 2001; pp. 11.1−11.55.
(22) Manzano Martínez, A. N.; Assirelli, M.; van der Schaaf, J. Droplet Size and Liquid-Liquid Mass Transfer with Reaction in a Rotor-Stator Spinning Disk Reactor. *Chem. Eng. Sci.* **2021**, *242*, 116706.
(23) de Beer, M. M.; Keurentjes, J. T. F.; Schouten, J. C.; Van der Schaaf, J. Engineering Model for Single-Phase Flow in a Multi-Stage Rotor-Stator Spinning Disc Reactor. *Chem. Eng. J.* **2014**, *242*, 53−61.
(24) Meeuwse, M.; van der Schaaf, J.; Schouten, J. C. Multistage Rotor-Stator Spinning Disc Reactor. *AIChE J.* **2012**, *58*, 247−255.

https://doi.org/10.1021/acs.iecr.1c02626
Ind. Eng. Chem. Res. 2021, 60, 15540−15548